A Three-Level Flying-Capacitor Rectifier Based Supercapacitor Direct Integration Scheme for Distributed Generation Systems

D.M. Vilathgamuwa, *Senior Member*, *IEEE*, S.D.G. Jayasinghe, *Student Member*, *IEEE*
School of Electrical & Electronic Engineering, Nanyang Technological University, Singapore
E-mail: emahinda@ntu.edu.sg, shan0034@ntu.edu.sg

***Abstract*-Supercapacitors are increasingly used as short term energy storage elements in distributed generation systems. The traditional approach in integrating them to the main system is the use of interfacing dc-dc converters which introduce additional costs and power losses. This paper therefore, presents a novel direct integration scheme for supercapacitors and thereby eliminates associated costs and power losses of interfacing converters. The idea is simply to replace ordinary capacitors of three-level flying-capacitor rectifiers with supercapacitors and operate them under variable voltage conditions. An analysis on the reduction of power losses by the proposed system is presented. Furthermore, supercapacitor sizing and implementation issues such as effects of the variable voltage operation and resistive behavior of supercapacitors at high frequencies are also discussed. Simulation results are presented to verify the efficacy of the proposed system in suppressing short term power fluctuations in wind generation system.**

I. INTRODUCTION

The contribution of electric power generation from renewable energy sources is getting significantly increased due to the concerns of depletion of fossil fuels and their greenhouse gas emissions. However, intermittency and scattered nature are the major challenges to be addressed in large scale integration of renewable sources such as wind, tidal and solar [1]. Distributed generation with wind, solar and diesel hybrid systems, as shown in Fig. 1(a), has been proposed as a promising solution for aforementioned issues [2]-[4]. In such systems, diesel generator is supposed to compensate power fluctuations caused by random changes in wind and solar irradiance.

Generally, solar irradiance varies at a slow rate and thus diesel generator can easily track its changes. But, wind has both short term and long term fluctuations and only the latter can accurately be compensated by diesel generators [5]-[7]. As a result, short term fluctuations are passed into the dc-bus and that create serious stability issues. The solution to this problem is the use of energy storage systems with high power transfer capability [8].

Supercapacitors are becoming the popular choice for implementing such energy storage systems due to their high power density, low standalone loss, long cycle life with no maintenance and nonexistence of toxic materials. The simplest way of incorporating a supercapacitor bank is the direct connection to the common dc-bus. But it suffers from several drawbacks such as limited voltage range, fixed current distribution governed by internal resistors and limited control over the power flow [9]. Effects of these issues can be reduced by placing an interfacing dc-dc converter between the supercapacitor and the dc-bus as shown in Fig. 1(a).

This dc-dc converter should possess the bidirectional power flow capability and thus it requires at least two fast switching devices rated to the peak power as shown in Fig. 1(b). Such converters introduce additional switching and conduction power losses. They also pose stability issues, particularly at high inrush currents [10]. Furthermore, interfacing converters add cost and weight to the system, mainly with their large inductors rated for the peak power transfer, which would be absent if a direct integration scheme with adequate controllability is available.

This paper therefore, presents a new direct integration scheme for supercapacitors using the generator-side converter. The proposed converter system is shown in Fig. 1(c) where the conventional flying-capacitors are replaced with three supercapacitor banks. This arrangement eliminates the need for interfacing dc-dc converters and thereby removes associated costs and power losses. In order to assess the efficiency improvement of the proposed system a comparison with the conventional dc-dc converter based approach is presented in this paper. Moreover, discussions on supercapacitor sizing, implementation issues and challenges due to supercapacitor voltage variations are also presented.

II. SYSTEM MODELING

A. Wind turbine power generation model

Power captured by the wind turbine can be expressed as in (1) [11].

$$P_m = 0.5\rho A C_p v_w^{\,3} \tag{1}$$

$$C_p(\lambda,\beta) = 0.73\left(\frac{151}{\lambda_i} - 0.58\beta - 0.002\beta^{2.14} - 13.2\right)\exp\left(\frac{-18.4}{\lambda_i}\right) \tag{2}$$

$$\lambda_i = \left[\frac{1}{(\lambda - 0.02\beta)} - \frac{0.003}{(\beta^3 + 1)}\right]^{-1} \tag{3}$$

$$\lambda = \frac{r\omega_m}{v_w} \tag{4}$$

where P_m is the captured wind power, ρ is the air density, A is the area swept by the turbine blades, C_p is the power coefficient, v_w is the wind speed, β is the blade pitch angle, λ is the tip speed ratio, r the turbine radius and ω_m is the mechanical angular frequency of the generator.

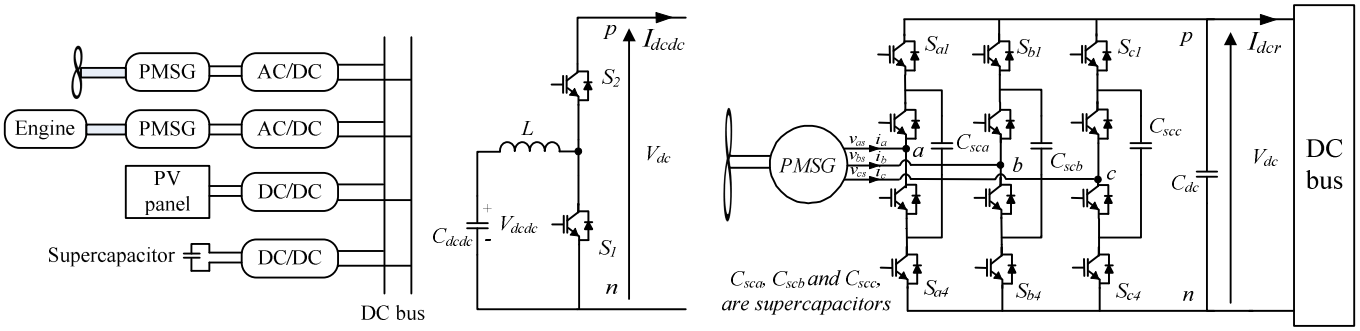

Fig. 1. (a) Distributed generation system with a common dc-bus, (b) bidirectional dc-dc converter, (c) proposed flying-capacitor rectifier with supercapacitor direct integration.

B. Generator model

The permanent magnet synchronous generator (PMSG) model in the synchronous reference frame is shown in Fig. 2. Based on this model, two expressions can be derived for *d-q* axis voltages as in (5) and (6) respectively [12].

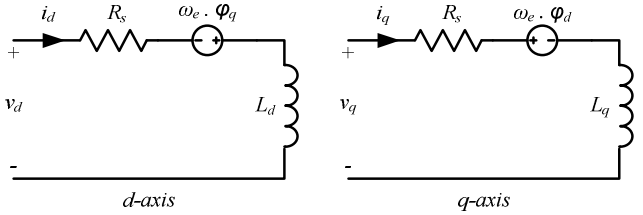

Fig. 2. PMSG model in the synchronous reference frame.

$$v_d = i_d R_s - \omega_e \varphi_q + L_d \frac{di_d}{dt} \tag{5}$$

$$v_q = i_q R_s + \omega_e \varphi_d + L_q \frac{di_q}{dt} \tag{6}$$

where v_d and v_q are *d-q* axis voltages, i_d and i_q are *d-q* axis currents, R_s is stator resistance, L_d and L_q are *d-q* axis inductances and ω_e is electrical rotational speed. φ_d and φ_q are magnetic flux components in *d-q* axes and their magnitudes are determined using (7) and (8). φ_m in (7) is the flux produced by permanent magnets of the generator. Electric torque produced by the generator is given by (9) where p is the number of pole pairs.

$$\varphi_d = L_d i_d + \varphi_m \tag{7}$$

$$\varphi_q = L_d i_q \tag{8}$$

$$T_e = \frac{3}{2} p\left(\phi_d i_q - \varphi_q i_d\right) \tag{9}$$

C. Supercapacitor model

The dynamic model of the supercapacitor can be represented by a capacitor and a series resistor as shown in Fig. 3. Both the capacitance and the series resistance of the supercapacitor vary with the frequency, temperature and voltage [13]. However, to avoid complexities and difficulties in simulation the effects of frequency, temperature and voltage variations are neglected and therefore the model consists of a constant capacitor and a series resistor.

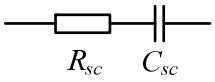

Fig. 3. Dynamic model of the supercapacitor.

III. Energy Management and Generator Controller

A. Generator controller

A simplified block diagram of the generator controller is shown in Fig. 4 where the measured wind speed is used to derive the reference speed. Actual generator speed is compared with the reference and the error is then passed into a PI controller which generates a reference for the *q*-axis component of the stator current. The *d*-axis component is maintained at zero.

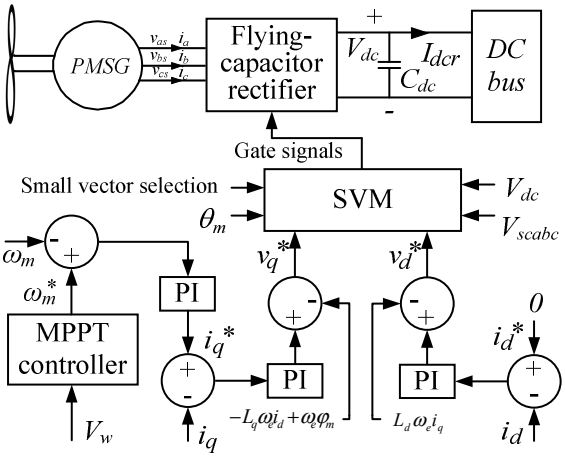

Fig. 4. Block diagram of the generator controller.

B. Energy management

It is proven in [14] that a half of the small vectors of the flying capacitor converter contribute for supercapacitor charging while the other half tend to discharge supercapacitors. Therefore, with the proper selection of small vectors it is possible to control supercapacitor charging and discharging. The energy management strategy of the

proposed system is based on this phenomena and the corresponding controller block diagram is shown in Fig. 5. The *q*-axis reference current is passed through a low pass filter (LPF) [15] to obtain a reference to the dc-link current, I_{dcr}. This reference is compared with the actual dc-link current and the error is then passed through a PI controller to obtain the duty cycle, SV_{ref}, for the subsequent PWM unit. The output of the PWM unit is either '0' or '1' which corresponds to charge and discharge respectively. Modulation algorithm uses this information to choose suitable small vector and thereby charge or discharge supercapacitors. This controller assumes an infinite dc-bus with regulated voltage, V_{dc}.

Energy management of the conventional approach with a bidirectional dc-dc converter is slightly different to the above. In this controller both charging and discharging small vectors are used at equal rate by setting the duty cycle reference, SV_{ref}, to 0.5. A separate controller, shown in Fig. 6, is used to derive switching signals for the dc-dc converter. Similar to the aforementioned controller this also uses the low pass filtered *q*-axis current reference to generate a reference for the dc-dc converter current. This reference is compared with the actual current and the error is passed through two PI controllers which separately drive the two switches in the dc-dc converter depending on the sign of the current error. The corresponding logic is expressed in (10).

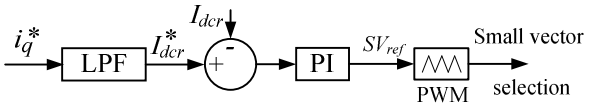

Fig. 5. Block diagram showing the energy management strategy of the proposed system.

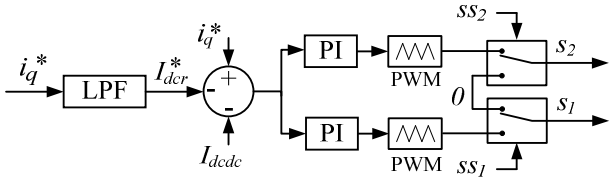

Fig. 6. Controller clock diagram of the dc-dc converter.

$$SS_x = \begin{cases} 0 & i_q^* > I_{dcr}^* \\ 1 & i_q^* \le I_{dcr}^* \end{cases} \quad x = 1,2 \tag{10}$$

IV. Power Losses in Switching Devices

In the proposed system IGBTs are used as switching devices. Their power losses are threefold, namely: turn on loss, turn off loss and conduction loss. The first two are known as switching losses and vary with the switching frequency while the last one varies with the duty cycle. Mathematical modeling of the three losses are given below.

A. Turn on loss

A typical turn on characteristic of an IGBT is shown in Fig 7 which consists of six steps. However, these six steps make the turn on loss calculation very complicated. Therefore, as shown by the red color lines in Fig. 7, a three step approximation is used in the derivation of the expression in (11) for the turn on loss.

$$E_{on} = (t_a + t_b) V_{CE} \frac{I_c}{2} \tag{11}$$

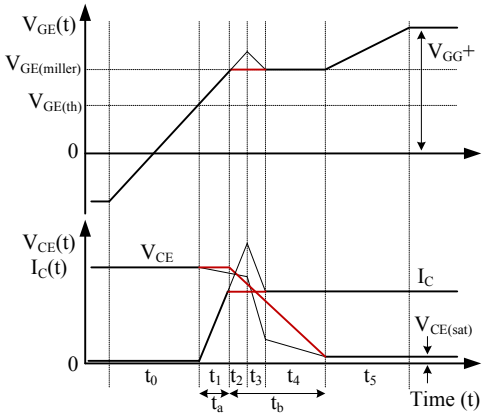

Fig. 7. IGBT turn-on characteristic and approximation.

B. Turn off loss

The turn off characteristic shown in Fig. 8 consists of five steps which make the turn off loss calculation is also complicated. Therefore, a three step approximation is used in the derivation of the expression in (12) for the turn off loss as well. The corresponding approximation is shown in Fig. 8 with red color lines.

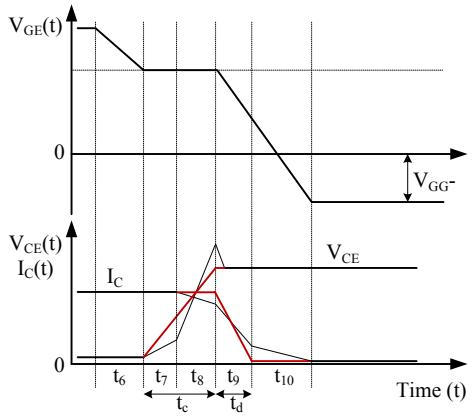

Fig. 8. IGBT turn-off characteristic and approximation.

$$E_{off} = (t_c + t_d) V_{CE} \frac{I_c}{2} \tag{12}$$

C. Conduction loss

The conduction loss of an IGBT occurs due to the on-state voltage drop which consists of two parts. One is the voltage drop, V_{sem}, of the drift region and the other is the ohmic drop due to the resistance of bonding wires and the substrate. The corresponding mathematical model is given in (13).

$$P_{con} = I_{c,avg} V_{sem} + I_{c,rms}^2 R_{bulk} \tag{13}$$

The total energy loss in one cycle is given in (14) where t_{cond} is the conduction time of the IGBT.

$$E_{total} = E_{on} + E_{off} + P_{con} t_{cond} \quad (14)$$

V. SUPERCAPACITOR SIZING AND IMPLEMENTATION ISSUES

A. Supercapacitor Sizing

The main cause of power fluctuations is the change of wind speed. Therefore, capacity of the energy storage system is also a function of the wind speed variation. In order to analyze this relationship wind is modeled as the sum of a dc quantity and a series of harmonics as in (15) [12]. In the following simulation wind speed fluctuation is assumed to be 8.75% of the mean value as in (16) which gives about 30% fluctuation in the captured wind power *P(t)*.

$$v_w(t) = V_{w0} + \sum \Delta V_{wi} \sin(\omega_i t) \quad (15)$$

$$v_w(t) = 8 + 0.7 \sin(2\pi t) \quad (16)$$

Power fluctuations caused by the above wind speed change have to be compensated by the energy storage system. Therefore, the required capacity of the supercapacitor bank is determined according to (17) and (18).

$$E_{sc,disch\,arg\,e} = \int_{0.5}^{1} P(t)dt - \frac{P_{out}}{2} \quad (17)$$

$$C_{sc} \geq \frac{2E_{sc,disch\,arg\,e}}{\left(V_{sc,H}^{\ 2} - V_{sc,L}^{\ 2}\right)} \quad (18)$$

where P_{out} is the power delivered to the dc-bus, $V_{sc,H}$ is the upper threshold of the supercapacitor voltage and $V_{sc,L}$ is the lower threshold of the supercapacitor voltage.

B. Implementation issues

In order to acquire the full benefit of supercapacitors their voltages are allowed vary within the range of $V_{dc}/3$, to $2V_{dc}/3$. This variable voltage operation creates three major problems. Unequal blocking voltages and increased voltage slew rates (dv/dt) experienced by some of the switching devices of the rectifier is the first issue. However, the rapid development of device technologies enables the use of such devices with increased blocking voltage and slew rate and hence this would not be a significant issue. The second problem is the unequal distribution of instantaneous power losses among switching devices. This causes some devices to be heated up more than the others. However, supercapacitor banks are used only as short-term power smoothening elements and hence their average power in a cycle is theoretically zero. That means, on average, power losses get distributed evenly among switching devices. Therefore, in steady state, temperatures of switching devices vary at the same rate. However, heat sinks should have enough capacity to protect devices from aforementioned instantaneous power losses.

The third problem is the uneven distribution of space vectors. When the supercapacitor voltages are equal to the half of the dc-link voltage the proposed system acts as a conventional three-level rectifier and the corresponding space vector distribution is shown in Fig. 9(a). If supercapacitor voltages are reduced to one third of the dc-link voltage, each leg of the inverter can produce four different voltage levels (0, $V_{dc}/3$, $2V_{dc}/3$ and V_{dc}). Therefore, in this case, the same system operates as a four-level rectifier with the space vector distribution as shown in Fig. 9(b). In order to differentiate each and every vector point, particularly when they overlap, slight changes have been introduced to supercapacitor voltages. Similarly, if supercapacitor voltages are increased to two third of the dc-link voltage each leg of the rectifier produces same voltage levels (0, $V_{dc}/3$, $2V_{dc}/3$ and V_{dc}). Therefore, the system again operates as a four-level rectifier in this case too. The corresponding space vector distribution looks very similar to Fig. 9(b). However, positions of some of the vectors get interchanged [14]. When supercapacitor voltages vary from $V_{dc}/3$, to $2V_{dc}/3$ the inner most hexagon shown in Fig. 9(b), expands while the other inner hexagon shrinks. When the voltages reach $V_{dc}/2$ both inner hexagons get overlapped as shown in Fig. 9(a). Further increase in supercapacitor voltage causes the expansion and shrinking of inner hexagons which eventually interchanges the two inner hexagons shown in Fig. 9(b). The end result of these variations is the uneven distribution of space vectors of the flying capacitor rectifier.

Conventional modulation methods fail to produce undistorted outputs under such dynamic situations. Authors have proposed a novel space vector modulation technique and capacitor voltage equalization algorithm in [14] which can produce undistorted outputs even in the presence of unevenly distributed space vectors. The same modulation technique and voltage equalization strategy are used for this system as well.

Supercapacitors behave as resistors at high frequencies (typically beyond few tens of Hz) [13]. Therefore, proposed system requires electrolytic capacitors to assist supercapacitors at high frequencies.

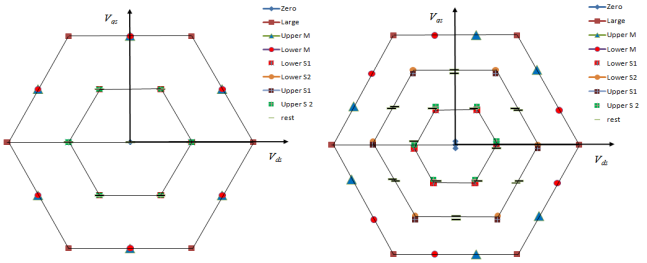

(a) (b)

Fig. 9. Space vector distribution at different supercapacitor voltage conditions (a) $V_{sca} = V_{scb} = V_{scc} = V_{dc}/2$, (b) $V_{sca} = 0.33V_{dc}$, $V_{scb} = 0.31V_{dc}$, $V_{scc} = 0.35V_{dc}$.

VI. SIMULATION RESULTS

Computer simulations were carried out on the MATLAB/SIMULINK/PLECS platform to compare the performance of the proposed direct integration scheme against the dc-dc converter based approach. Results obtained through these simulations are shown in Fig. 10 where the waveforms in the left correspond to the separate dc-dc converter based approach and the results in the right are for

the proposed scheme. System parameters of both simulation setups are given in Table I. The wind speed profile shown in Fig. 10(a and b) is used in both simulations. The corresponding power variations are shown in Fig. 10(c and d) where both systems are controlled in a way that a regulated power, P_{out}, is delivered to the dc-bus irrespective of the fluctuations present at the input.

In the dc-dc converter based system the supercapacitor attached to the converter is used to absorb power fluctuations and the capacitors of the rectifier are used to perform the usual clamping operation. The corresponding capacitor voltage variations are shown in Fig. 10(e). In this figure the waveform marked as V_{dcdc} represents the voltage of the supercapacitor attached to the dc-dc converter which shows an increase when there is a surplus of power and a decrease for deficit of power. The clamping capacitors are maintained at the half of the dc-link voltage. Operation of the proposed system is opposite to that where the voltage of clamping capacitors are allowed to vary as shown in Fig. 10(f). This variation is similar to the supercapacitor voltage variation shown in Fig. 10(e) which confirms the ability of the proposed system to interface supercapacitor energy storage systems. The corresponding current variations are shown in Fig. 10(g and h). In these diagrams the waveform marked with I_{dc} represents the current injected into the dc-bus which remains nearly constant all the time. The waveform marked with I_{dcr} represents the output current of the rectifier while the waveform marked with I_{dcdc} represents output current of the dc-dc converter.

In the dc-dc converter based system fluctuations present in the rectifier current are compensated by the output current of the dc-dc converter as shown in Fig. 10(g). Furthermore, average currents of the clamping capacitors are zero which indicate a zero energy storage within the rectifier. This is achieved by setting the duty cycle of the small vector selection unit to 0.5 as shown in Fig. 10(i) which in turn selects both charging and discharging small vectors at an equal rate. But in the proposed system clamping capacitors are used to absorb power fluctuations and thus the average capacitor current is not zero as shown in Fig.10(h). The corresponding variation of the small vector duty cycle is shown in Fig. 10(j).

The most important result obtained through these simulations is the comparison of energy loss between the dc-dc converter based system and the proposed system as shown by the waveforms in Fig. 10 (k) and Fig. 10(l) respectively. According to these two figures energy loss within the rectifier is same for both systems. In other words, the proposed direct integration feature does not bring additional losses to the rectifier. Furthermore, it eliminates the losses associated with the dc-dc converter and thereby confirms the efficacy of the proposed direct integration scheme in terms of power loss reduction. Moreover, the variable voltage operation of supercapacitors does not make significant impacts on the input voltage and phase currents as shown by the waveforms in Fig. 10(m to q)

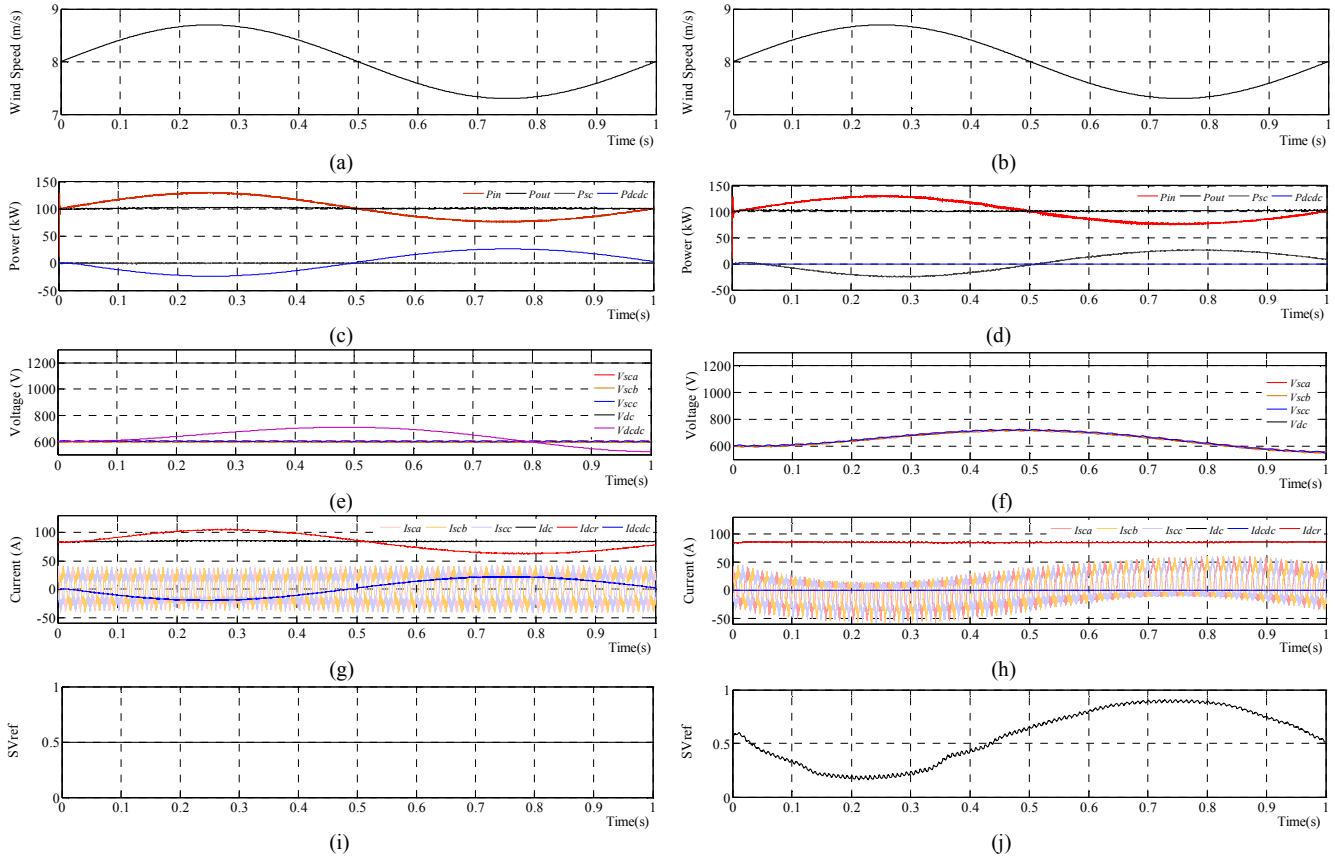

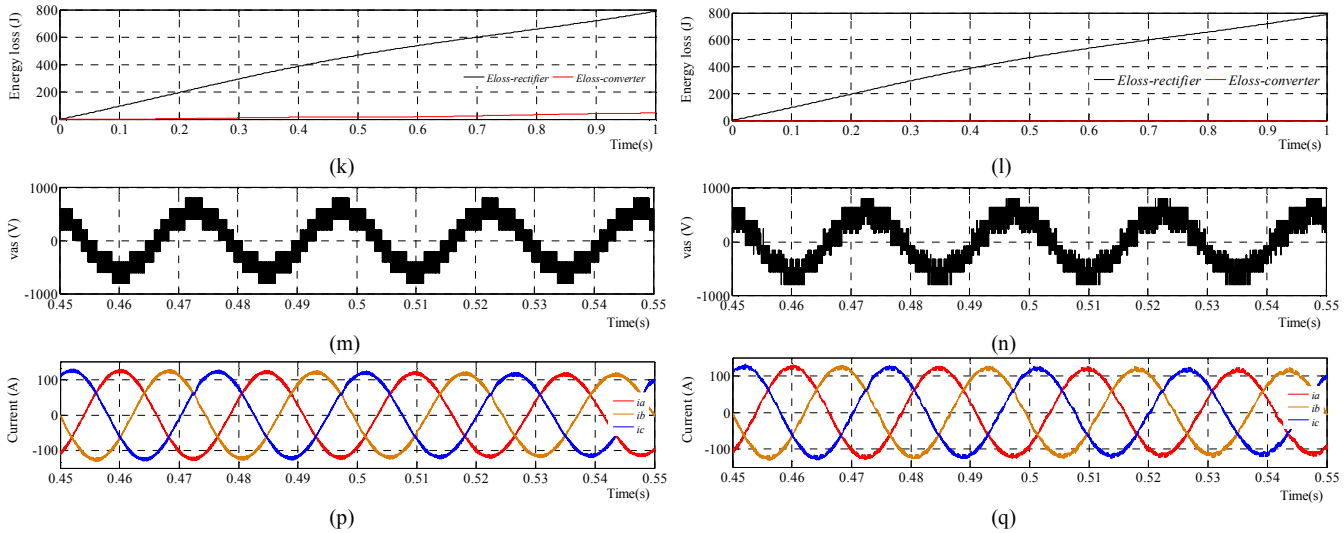

Fig. 10. Comparison between the dc-dc converter based approach (waveforms on the left) and the proposed system (waveforms in the right) (a) (b) wind speed, (c) (d) input, output and supercapacitor power, (e) (f) supercapacitor voltage variations, (g) (h) rectifier output current, dc-dc converter current, clamping capacitor current (filtered) and the current injected into the dc-bus, (i) (j) control signal for small vector selection, (k) (l) Energy loss within the rectifier and the dc-dc converter, (m) (n) *a*-phase voltage at the input of the rectifier, (p) (q) phase currents.

VII. CONCLUSIONS

A three-level flying-capacitor rectifier based supercapacitor direct integration scheme is proposed for distributed generation systems feeding a common dc-bus. The disposal of dc-dc converter in interfacing supercapacitors eliminates associated costs and power losses. In order to get the optimum use of supercapacitors in the proposed scheme, they are operated under variable voltage conditions. The challenges of this variable voltage operation and possible solution are discussed. Supercapacitor sizing and implementations issues are also discussed in detail. Simulation results are presented to prove the efficacy of the proposed direct integration scheme against the conventional dc-dc converter based approach.

TABLE I. SYSTEM PARAMETERS OF THE SIMULATION SETUP

Fundamental frequency	f = 50Hz
Switching frequency of the rectifier	f_{sr} = 5kHz
Switching frequency of the dc-dc converter	f_{sdcdc} = 15kHz
Capacitance of supercapacitors	C_{scx} = 30mF
Range of supercapacitor voltage	V_{scx} = 400-800V
DC-Link voltage	V_{dc} = 1200V
Resistance of the PMSG	R = 0.2Ω
Inductance of the PMSG	L = 1mH
Rated power of the PMSG	200kW

REFERENCES

[1] H. Nehrir, C. Wang, K. Strunz, H. Aki, R. Ramakumar, J. Bing, z. Miao, and Z. Salameh, "A Review of Hybrid Renewable/Alternative Energy Systems for Electric Power Generation: Configurations, Control and Applications," *IEEE Trans. Sust. Energy*, Vol.2, no.4, pp.392-403, Oct. 2011.

[2] P. Siano, C. Citro, C. Cecati, and A. Piccolo, "Smart Operation of Wind Turbines and Diesel Generators According to Economic Criteria," *IEEE Trans. Ind. Electron.*, vol. 58, no. 10, pp. 4514-4525, Oct. 2011.

[3] R. S. Fernandez, "Simulation of the transition from Wind only mode to Wind Diesel mode in a no-storage Wind Diesel System," *IEEE Trans. Latin America*, vol.7, no.5, pp.539-544, Sept. 2009.

[4] C. Abbey, and G. Joos, "A Stochastic Optimization Approach to Rating of Energy Storage Systems in Wind-Diesel Isolated Grids," *IEEE Trans. Power Systems*, vol.24, no.1, pp.418-426, Feb. 2009.

[5] R. Pena, R. Cardenas, J. Proboste, J. Clare, and G. Asher, "Wind–Diesel Generation Using Doubly Fed Induction Machines," *IEEE Trans. Energy Convers.*, vol.23, no.1, pp.202-214, March 2008.

[6] A. M. O. Haruni, A. Gargoom, M. E. Haque, and M. Negnevitsky, "Dynamic operation and control of a hybrid wind-diesel stand alone power systems," in *Proc. Applied Power Electronics Conference and Exposition*, APEC 2010 pp.162-169, 21-25 Feb. 2010.

[7] N. Mendis, K. M. Muttaqi, S. Sayeef, and S Perera, "A control approach for voltage and frequency regulation of a Wind-Diesel-battery based hybrid remote area power supply system," in *Proc. IEEE Ind. Electron. Society Conf., IECON 2010*, pp.3054-3060, 7-10 Nov. 2010.

[8] T. Hirose, and H. Matsuo, "Standalone Hybrid Wind-Solar Power Generation System Applying Dump Power Control without Dump Load," *IEEE Trans. Ind. Electron.*, vol.59, no.2, pp.988-997, Feb. 2012.

[9] S. D. G. Jayasinghe, D. M. Vilathgamuwa, and U. K. Madawala, "A Hybrid Cascaded Multilevel Inverter with Supercapacitor Direct Integration for Wind Power Systems." in *Proc. Intl. Conf. on Power Electron., ICPE 2011*, June 2011.

[10] Shuai Lu, K. A. Corzine, and M. Ferdowsi, "A Unique Ultracapacitor Direct Integration Scheme in Multilevel Motor Drives for Large Vehicle Propulsion," *IEEE Trans. Veh. Tech.*, vol. 56, no. 4, pp. 1506-1515, July 2007.

[11] V. Agarwal, R. K. Aggarwal, P. Patidar, and C. Patki, "A Novel Scheme for Rapid Tracking of Maximum Power Point in Wind Energy Generation Systems," *IEEE Trans. Energy Convers.*, vol.25, no.1, pp.228-236, March 2010.

[12] T. H. Nguyen, D. C. Lee, S. Seung-Ho, and E. H. Kim, "Improvement of power quality for PMSG wind turbine systems," in *Proc. IEEE Energy Conversion Congress and Exposition, ECCE 2010*, pp.2763-2770, 12-16 Sept. 2010.

[13] W. Lajnef, J. M. Vinassa, O. Briat, S. Azzopardi, and C. Zardini, "Study of ultracapacitors dynamic behavior using impedance frequency analysis on a specific test bench," in *Proc. IEEE Intl. Sympo. On Ind. Electron.*, pp. 839- 844 vol. 2, 4-7 May 2004.

[14] S. D. G. Jayasinghe, D. M. Vilathgamuwa, and U. K. Madawala, "An analysis on the possibility of using capacitors of a three-level capacitor clamped inverter as power smoothing elements for wind power systems," in *Proc. IEEE Energy Conversion Congress and Exposition, ECCE 2011*, pp.2963-2970, 17-22 Sept. 2011.

[15] S. M. Muyeen, R. Takahashi, T. Murata and J. Tamura, "Integration of an Energy Capacitor System With a Variable-Speed Wind Generator," *IEEE Trans. Energy Convers.*, vol. 24, no. 3, pp. 740-749, Sep. 2009.